Polymer 51 (2010) 6278–6283

Contents lists available at ScienceDirect

Polymer

journal homepage: www.elsevier.com/locate/polymer

Correlation between structural and dynamic mechanical transitions of regenerated silk fibroin

Qingqing Yuan, Jinrong Yao, Lei Huang, Xin Chen, Zhengzhong Shao*

The Key Laboratory of Molecular Engineering of Polymers of MOE, Department of Macromolecular Science, Laboratory of Advanced Materials, Fudan University, Shanghai 200433, PR China

ARTICLE INFO

Article history:
Received 23 March 2010
Received in revised form
17 September 2010
Accepted 25 October 2010
Available online 30 October 2010

Keywords:
Glass transition
Semicrystalline
Disordered domain

ABSTRACT

Dynamic mechanical analysis (DMA) was applied to investigate the correlation between dynamic mechanical behaviors of regenerated silk fibroin (RSF) and its structural transition which was characterized by near-infrared (NIR) spectroscopy. The tan δ peak split of DMA demonstrated that the apparent glass transition of amorphous RSF film (at around 177 °C) was the contribution of both uncrystallizable and crystallizable segments through homogeneous amide–amide hydrogen bonds, which were gradually separated from each other and produced disordered and β-sheet domains during ethanol treatment. Furthermore, DMA was also applied as "thermal fingerprint" to investigate water effect on the disordered domains of silk fibroin. The results showed that glass transition temperature of permanently disordered domains in crystallized RSF films was increased from 155 °C to 190 °C after thermal dehydration, and even approached 205 °C for stretched RSF films.

1. Introduction

The relationship between structure and performance is an essential issue in material science. Silk fibroin, after application in textile industry for centuries, has recently been extensively utilized in non-textile fields such as fiber composite, 3D scaffold, electrospun nonwoven, optical element and drug capsule, etc. [1–3]. Analogous to classical semicrystalline polymers, it structurally consists of hydrophobic segments of repetitive GAGAGS, and hydrophilic segments of polar, charged or bulky side-chain amino acids [4,5]. The highly periodic GAGAGS segments tend to stack into anti-parallel β-sheets, known as ordered domains (or so called "crystalline domains"), while those less periodic hydrophilic segments tend to form random coil, helix or β-turn conformations that are all assigned to disordered domains [1,6,7]. In fact, the fabrication of silk fibroin-based materials is a process technically involving a transition from soluble structure (dominated by so called Silk I [2]) to insoluble Silk II structure (dominated by β-sheets) or vice versa. Structural transitions of silk fibroin like crystallization or orientation occur only above the glass transition temperature (T_g) when molecular backbone obtains sufficient motility to reorganize into more stable and ordered structure [8,9]. On the other hand, fine structure of silk fibroin also determines the overall properties of its end-products, such as required mechanical performance, controllable degradation rate or specific material morphology, etc. [9–11]. Therefore, it is crucial to understand the glass transition of silk fibroin and its correlation with the fine structure, across various regenerated silk fibroin (RSF) formats such as fiber, scaffold, nonwoven mat, film, particle, etc.

Dynamic mechanical analysis (DMA) technique has been extensively applied to investigate the viscoelasticity features (including T_g) of solid materials. Firstly, although T_g is often determined by DSC, heat capacity of silk proteins [12–14] is sometimes too tricky to be calculated. Nevertheless, DMA is sensitive to glass transition because the storage modulus decreases in a 3–4 order of magnitude at T_g, along with a loss modulus peak and a loss tangent peak (tan δ) as well. Secondly, the multiple operation modes of DMA test can satisfy the growing variety of RSF formats. Thirdly, DMA may facilitate material measurement by simultaneously providing information of both molecular chain movement and bulky mechanical properties. As a result, DMA has been successfully applied to study the dynamic mechanical properties of silk fibroin [13,15–20], and the compatibility of silk fibroin with chitosan and cellulose [21], etc.

It is widely demonstrated that the apparent glass transition of silk fibroin occurred at about 175–180 °C in predominantly amorphous structure (either regenerated from fibroin solution [8,13] or obtained from silk gland [22–24]) and around 220–230 °C in highly ordered structure (i.e. silk fiber [25,26]), though the T_g value

* Corresponding author. Tel.: +86 21 65642866; fax: +86 21 65640293.
E-mail address: zzshao@fudan.edu.cn (Z. Shao).

0032-3861/$ – see front matter © 2010 Elsevier Ltd. All rights reserved.
doi:10.1016/j.polymer.2010.10.046

determined by different tools might be slightly variant. However, the understanding underlying glass transition and different fine structures remains still obscure. For example, even though both sampled after methanol-induced crystallization, Tsukada et al. [12] reported glass transition of silk fibroin membrane at 183 °C by thermal dilatometer, while Magoshi et al. [27] observed the same glass transition at a higher temperature (above 195 °C) by DMA. Similarly, even though both sampled after thermal dehydration, Magoshi et al. [27] also detected two endothermic shifts of silk fibroin film at 175 °C and 185 °C after preheating at 100 °C by DSC, while Motta et al. [13] detected a single loss modulus peak shifted from 167 to 180 °C in the first and second DMA temperature scan (ranging up to 200 °C). Water effect could be one possible reason for those disparities, i.e., the procedure of dehydration has a strong influence on glass transition of silk fibroin.

In this paper, DMA technique was applied to identify the dynamic mechanical behaviors of RSF films during ethanol-induced crystallization from random coil/helix to β-sheet structure. The tan δ results demonstrated that, as an alternative for common characterization method like near-infrared (NIR) spectroscopy, DMA was an effective tool for the insight of particular structure in crystallized RSF films. Furthermore, DMA was also applied as "thermal fingerprint" to investigate structural changes of RSF films after thermal dehydration, which could help the understanding of structural refinement of RSF materials such as annealed artificial fiber [28,29] and post-stretched film [20].

2. Experimental section

2.1. Sample preparation

Air-cast RSF films. The 7 wt% RSF aqueous solution was obtained according to established procedures [30], and was cast on polystyrene disks to dry overnight at room temperature and 50 ± 5% relative humidity (RH). The obtained translucent, yellowish-white RSF films had a thickness of around 140 ± 20 μm, suitable for the penetration of alcohol [8] and both measurements of DMA and NIR spectroscopy [31]. Such air-cast RSF films contained amorphous structure confirmed by NIR spectra, and could be easily redissolved in deionized water.

Crystallized RSF films. Air-cast RSF films were immersed in 80% (v/v) ethanol solution for a series time of 2 min, 5 min, 10 min, 20 min, 60 min and 24 h, respectively. The films were then cut into 10 mm × 4 mm specimens with a razor blade, later vacuumed for 3 h and kept in a desiccator against P_2O_5. These crystallized RSF films had negligible water content after dehydration in vacuum, only 2.1 ± 0.2 wt% which was detected by TGA measurement.

Thermally dehydrated RSF films. Ethanol-treated RSF films were exposed to different RH for two weeks until humidity quasi-equilibrium, according to the method in literature [32]. Four approximate RH, i.e., 11%, 43%, 67% and 75%, were generated by saturated LiCl, K_2CO_3, $CuCl_2$ and NaCl aqueous solutions at 25 ± 2 °C, respectively. The average initial water content of hydrated RSF films under each RH was 6.0 ± 0.3 wt%, 10.1 ± 0.3 wt%, 12.0 ± 0.2 wt%, 13.8 ± 0.4 wt%, which were detected by TGA measurements. Then hydrated RSF films were isothermal at 130 °C to remove water thoroughly, and these thermally dehydrated RSF films were kept in a desiccator against P_2O_5.

Stretched RSF films. Air-cast RSF films were immersed in 80% (v/v) ethanol solution for 24 h, and then cut into 10 mm × 4 mm specimens with a razor blade. The films absorbed ethanol and were immediately drawn to three times of their initial length at a strain rate of 500%/min on an Instron 5565 universal test machine. The stretched RSF films were constrained at both ends before dry, then isothermal at 130 °C to remove water thoroughly and kept in a desiccator against P_2O_5.

2.2. Near-infrared measurement

For secondary structural characterization of RSF films, NIR spectroscopy has unique advantages over classical mid-infrared (MIR) spectroscopy, such as weak disturbance of moisture and less restriction of sample thickness [31,33]. Thus, NIR spectra of all as-prepared RSF films were collected in transmission mode using a Nicolet Nexus470 FT-IR spectrometer equipped with liquid nitrogen cooled MCT detector. The resolution of each spectrum was 4 cm^{-1}, 128 interferograms in a range of 4000–11,000 cm^{-1}.

2.3. Dynamic mechanical analysis

DMA measurement of all as-prepared RSF films was carried on a Netzsch 242 dynamic mechanical analyzer with a purging nitrogen gas of 20 mL/min, 1 Hz of frequency, 0.125% of strain and 3 °C/min of heating rate. The real-time temperature of the machine was calibrated by polyethylene terephthalate (PET) standard specimen. DMA measurement of degummed silk fibers was performed on Rheometric Scientific DMTA-IV with 1 Hz of frequency, 0.5% of strain and 3 °C/min of heating rate.

2.4. Thermogravimetric analysis

Derivative thermogravimetric (DTG) curves of ethanol-treated RSF films were examined up to 600 °C through a Perkin Elmer Pyris-1 thermogravimetric analyzer at a heating rate of 10 °C/min, with a purging nitrogen gas of 40 mL/min. Water content of both dehydrated and hydrated RSF films was also determined by the same machine as the weight loss after isothermal at 130 °C until weight change was within ±0.2%.

3. Results and discussion

Dynamic loss tangent (tan δ) curves of DMA are widely used to interpret molecular movement of polymers and the resulted changes in structure. For example, Guadagno et al. [34,35] analyzed structural and dynamic mechanical behaviors of different syndiotactic polypropylene (PP) polymorphs, and successfully correlated structural transitions between PP polymorphs with distinctive tan δ curves observed by DMA. In this paper, tan δ curves of different types of RSF films were obtained to identify segmental movements of silk fibroin molecules in agreement with various structures resulted from crystallization, heating and orientation.

3.1. Characterizations on RSF films with ethanol-induced crystallization

Extensive studies had shown that alcohols could induce the crystallization of silk proteins from random coil/helix to β-sheet conformation [12,18,30]. Therefore, for the investigation of dynamic mechanical properties of RSF films with varying β-sheet content, air-cast RSF films were immersed in 80% (v/v) ethanol solution for 2 min to 24 h, and characterized by NIR spectroscopy firstly.

NIR spectrum of untreated air-cast RSF film showed a remarkable peak centered at 4605 cm^{-1} in the 4450–4480 cm^{-1} region (Fig. 1), which was previously ascribed to the combination band of amide A and amide III. It suggested a predominant conformation of random coil and/or helix in the untreated air-cast RSF films [31]. With the increase of immersion time in ethanol solution, the RSF films were observed a drop of absorption intensity at 4605 cm^{-1}, and a shoulder raised at 4525 cm^{-1} that was assigned to β-sheet conformation [31].

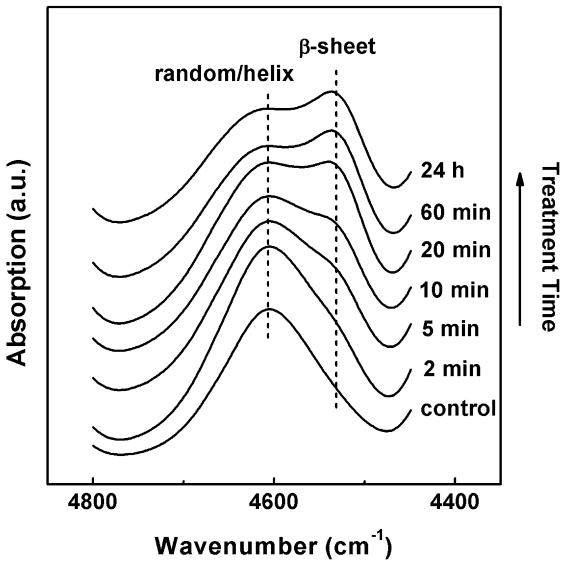

Fig. 1. NIR spectra of air-cast RSF films before (control) and after immersion in 80% (v/v) ethanol solution for 2 min to 24 h, respectively.

Thus, the NIR spectra revealed as expected the structural transition of RSF films from random coil/helix to β-sheet via ethanol treatment.

Typical DMA results of air-cast RSF film which contained amorphous structure was shown in Fig. 2A. The storage modulus (E') value remained almost constant as the temperature increased up to 150 °C, and then decreased rapidly as a result of thermal relaxation of fibroin backbone. After a short plateaus at about 200–230 °C, the storage modulus displayed another sharp fall at about 240 °C due to the beginning of thermal degradation of silk fibroin [13]. Correspondingly, the tan δ curve showed little change until at 150 °C where the tan δ peak began to appear and reached a maximum at 177 °C. This temperature of tan δ peak was taken as the T_g of amorphous RSF film and was consistent with literatures [8,13,22–24]. Using data from tan δ curves, we then analyzed RSF segmental movements via different treatments.

With the increase in the duration of ethanol treatment, the unique tan δ peak of air-cast RSF film at 177 °C gradually split into two peaks at lower and higher temperatures respectively (Fig. 2B), corresponding to the peak shifts observed in NIR spectra (Fig. 1). This low-temperature tan δ peak shifted from around 168 °C for the films treated with ethanol for 2–5 min, then to 161 °C for the film treated for 10 min, and relocated at around at 155 °C for all films treated longer than 20 min. The relative height of low-temperature tan δ peak first depressed with the increase of treatment time, and then remained almost constant for those films that were treated with ethanol for longer than 60 min, when the structural transition to β-sheet was almost complete (Fig. 1). Simultaneously, in the higher temperature region of the tan δ curves, a small shoulder peak (pointed by an arrow in Fig. 2B) appeared at 190 and 215 °C for the films treated with ethanol for 2 and 5 min, respectively. This high-temperature peak shifted to around 230 °C for the films treated for longer time and was accompanied with a sharp fall of tan δ due to the beginning of thermal degradation of silk fibroin at around 240 °C.

Considering the ethanol-induced β-sheet crystallization confirmed by NIR spectra, the tan δ peak constantly at about 155 °C suggested the presence of a distinctive structure in RSF films, different from β-sheet domains. The thermal relaxation of β-sheet domains of silk fibroin should appear at a higher temperature (i.e. above 200 °C) [8]. Also, the shifts of tan δ peak might not relate to water effect [32], because all samples were excessively dehydrated in vacuum against P_2O_5 and the average water content determined by TGA was only 2.1 ± 0.2 wt%. Therefore, the tan δ peak of RSF films at 155 °C should be related to the relaxation of permanently disordered domains (i.e. uncrystallizable segments) of silk fibroin with more free motility (vs. β-sheet domains). In our previous work on silk fiber/fibroin composite [36], a slight but broaden tan δ peak centered at 155 °C was also observed, which was demonstrated as the result of loosened fibroin segments produced by partial dissolution of silk fibers after a LiBr pretreatment. Furthermore, in our opinion, the tan δ peak at 155 °C was not shown up in untreated air-cast RSF film because the local environment of each fibroin chain was homogeneous, and the motility of uncrystallizable portions was limited by the hydrogen bonds between crystallizable and uncrystallizable segments. After ethanol treatment, those crystallizable segments stacked into β-pleats by breaking hydrogen bonds with the uncrystallizable ones, and a step-by-step microphase separation between the crystalline domains and intrinsically disordered domains took place [9]. Thus, a clear split of tan δ peak was observed and the tan δ peak of permanently disordered domains of silk fibroin appeared at around 155 °C.

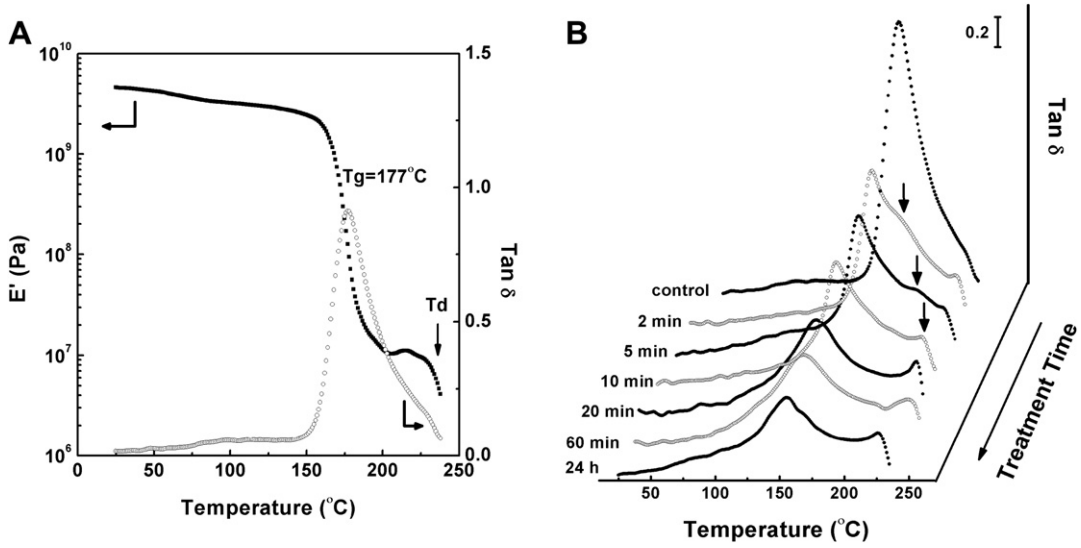

Fig. 2. DMA results of untreated air-cast RSF film (A) and tan δ curves of RSF films before (control) and after immersion in 80% (v/v) ethanol solution for 2 min to 24 h, respectively (B).

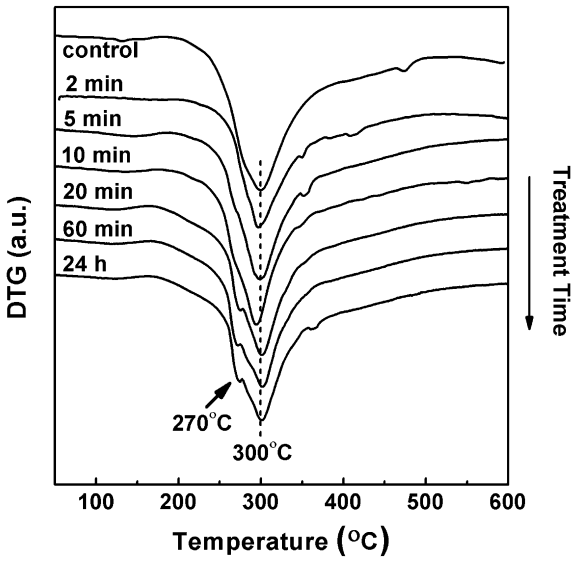

Fig. 3. DTG results of air-cast RSF films before (control) and after immersion in 80% (v/v) ethanol solution for 2 min to 24 h, respectively.

On the other hand, the tan δ peak at higher temperature was presumed to correlate to the newly formed β-sheet domains. This high-temperature tan δ peak, shifted from 190 °C to 215 and 230 °C as the structure changed from random coil/helix to β-sheet [13,22,27,37]. The tan δ peak at around 230 °C for RSF films that almost completed such transition, however, could be the result of β-sheet segmental relaxation along with simultaneous thermal break-ups of fibroin backbone.

DTG results provided further evidence for the suspected microphase separation between permanently disordered domains and β-sheet domains of silk fibroin. In Fig. 3, the maximum degradation rate occurred at around 300 °C for all RSF films. However, with the increase of β-sheet portions induced by ethanol, a shoulder showed up at a lower temperature around 270 °C, indicating a different degradation rate existed in the crystallized RSF films. Such a phenomenon was also observed by Magoshi et al. in their study of structural transition during the stretching of natural silk fibroin films (obtained directly from silk gland) [1]. Considering the thermal stability difference between disordered domains and β-sheet domains, the thermal instability shoulder at 270 °C could be attributed to the degradation of permanently disordered domains in crystallized RSF films.

3.2. Characterizations on RSF films with thermal dehydration

Many studies have demonstrated that water exerts a strong plasticizing action to hygroscopic polymers such as silk fibroin, causing a large reduction of their glass transition temperature and a noticeable mechanical transition from glassy to rubbery state as well [32,38–40]. On a molecular level, although closely packed β-sheet domains are immune to water, the disordered domains of silk fibroin are vulnerable to water plasticization. Therefore, water effect on dynamic mechanical behaviors of RSF films after ethanol treatment was further investigated under thermal dehydration condition. Two types of RSF films, which were previously immersed in 80% ethanol for 10 min (named **RSF-1**) and 24 h (named **RSF-2**) respectively, were used here for comparison in our study.

After the exposure to constant relative humidity ranging from 11% to 75% at room temperature, both **RSF-1** and **RSF-2** films had absorbed 6.0 wt% to 13.8 wt% water, respectively. But neither of the hydrated RSF films had experienced apparent secondary structural changes in humid environment as was revealed by NIR spectra (Supplementary material, Fig. S1). After isothermal at 130 °C to thoroughly remove water, the thermally dehydrated **RSF-1** films produced a drop of absorption intensity at 4605 cm^{-1} and a shoulder raised at 4525 cm^{-1} in NIR spectra with the increase of initial water content before heating (Fig. 4A). Since silk fibroin molecules had only partially crystallized after a short time of ethanol treatment, the NIR results of **RSF-1** films revealed the further secondary structural transition for β-sheets induced by heat. Increasing initial water content would help such secondary structural transition of **RSF-1** films, because β-sheet crystallization only occurred when the crystallizable segments of silk fibroin obtain sufficient motility (by water plasticization) and energy (by heat) [37]. In comparison, the thermally dehydrated **RSF-2** films that were previously treated with ethanol for 24 h, showed no apparent changes in NIR spectra (Fig. 4B). It indicated that almost all the crystallizable segments of silk fibroin in **RSF-2** films had already stacked into β-sheet domains as a result of long ethanol treatment.

As shown in Fig. 5, after complete thermal dehydration at 130 °C, the tan δ peak of **RSF-1** films shifted gradually from around 162 °C to 195 °C as the initial water content increased from 6.0 wt

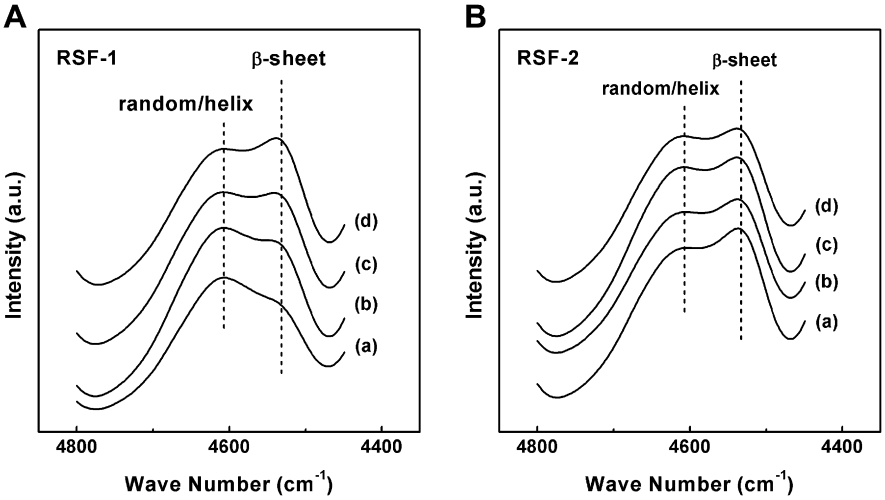

Fig. 4. NIR spectra of thermally dehydrated **RSF-1** (A) and **RSF-2** (B) films. Average water content of the films before heating was 6.0 wt%, 10.1 wt%, 12.0 wt%, 13.8 wt% (a–d), respectively.

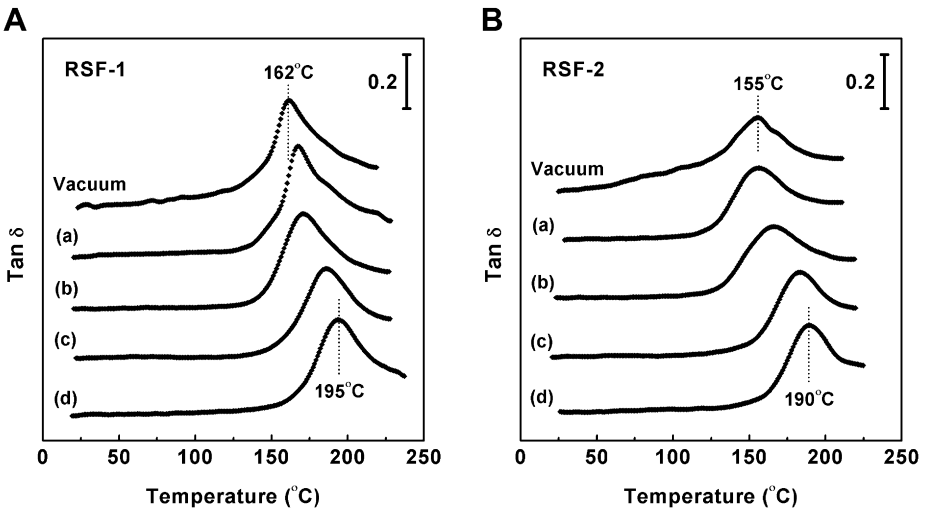

Fig. 5. Tan δ peak shift of thermally dehydrated **RSF-1** (A) and **RSF-2** (B) films. Average water content of the films before heating was 6.0 wt%, 10.1 wt%, 12.0 wt%, 13.8 wt% (a–d), respectively.

% to 13.8 wt%. For **RSF-2** films, the tan δ peak also shifted from around 155 °C to 190 °C. Despite of NIR spectra differences between **RSF-1** and **RSF-2** films (Fig. 4), the similar DMA results indicated that the shift of tan δ peak cannot be simply attributed to heat-induced secondary structural transition from random coil/helix to β-sheet [33]. Water effect (i.e. thermal dehydration) might be more important to the glass transition of silk fibroin. In our opinion, in a humid environment, water would form amide-water hydrogen bonds in those accessible disordered domains and prevent silk fibroin molecules from forming new β-sheet domains (Supplementary material, Fig. S1). The removal of water by thermal dehydration led to a reorganization of the disordered domains for more stable and ordered structure and simultaneous β-sheet crystallization of intrinsically crystallizable segments in these domains if possible. The higher water content in RSF films means the better improvement of segmental motility for such reconstruction of order. Therefore, the shift of tan δ peak to higher temperature with the increase of initial water content indicated a heat-induced 'hardening' behavior of hydrated RSF films. Moreover, the combination of DMA and NIR results also suggested that, rather than extremely increasing secondary structural transition for more β-sheet domains, post-transition treatments such as water annealing might be more crucial to the thermal and mechanical performance of RSF materials such as artificial fibers.

Furthermore, dynamic mechanical behaviors of stretched RSF films were studied for the suggestion that silk fibroin would reconstruct into a more ordered structure after thermal dehydration. It is well known that orientation is crucial to the thermal and mechanical performance of semicrystalline polymers [7,35], and stretching is a feasible method to induce highly ordered structure especially in fiber spinning process [28,29,41]. The DMA results in Fig. 6 showed that the tan δ peak of stretched RSF films was around 205 °C, which approached the T_g of silk fiber (219 °C). Therefore, it indicated that more ordered structure in silk fibroin might increase the T_g of disordered domains, which was consistent with the results obtained from the thermal dehydration on RSF films.

3.3. DMA characterization of disordered domains of silk fibroin

The glass transition is an important thermal parameter that correlates with distinctive microstructure in silk fibroin. However, as mentioned above, the T_g of silk fibroin was reported in a wide range of 150–250 °C by literatures, and the relationship between glass transition and microstructure of silk fibroin was still unclear. Because silk fibroin would undergo thermal degradation during melting (i.e. segmental movement of β-sheet domains), the dynamic relaxations of the disordered domains of silk fibroin via different treatments was appropriately characterized by DMA technique.

Four representative T_g of RSF films obtained from amorphous state, ethanol-induced crystallization, thermal dehydration and stretching-induced orientation were found to be at around 177 °C, 155 °C, 190 °C and 205 °C, respectively (Fig. 6). As shown in Scheme 1, the structural transitions of RSF were likely the results of following events: in amorphous state, the uncrystallizable (e.g. hydrophilic motifs) and crystallizable segments (e.g. reserving GAGAGS motifs) of silk fibroin molecules were interacted with each other by homogeneous amide-amide hydrogen bonds, which resulted in a unique T_g at 177 °C by limiting the motility of intrinsically uncrystallizable segments. During ethanol treatment, the crystallizable segments formed β-sheet domains, left those uncrystallizable segments as permanently disordered domains (T_g = 155 °C) via a microphase separation. Besides, water in the RSF films could plasticize and expand the accessible disordered domains in humid environment. These domains would be forced

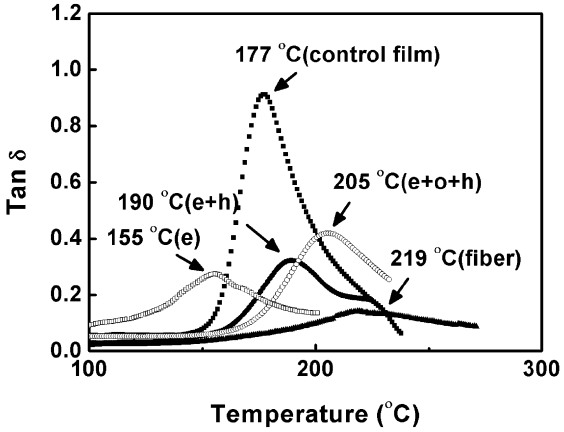

Fig. 6. Representative tan δ curves of RSF films with different structures (e: ethanol-induced crystallization; h: thermal dehydration; o: stretching-induced orientation).

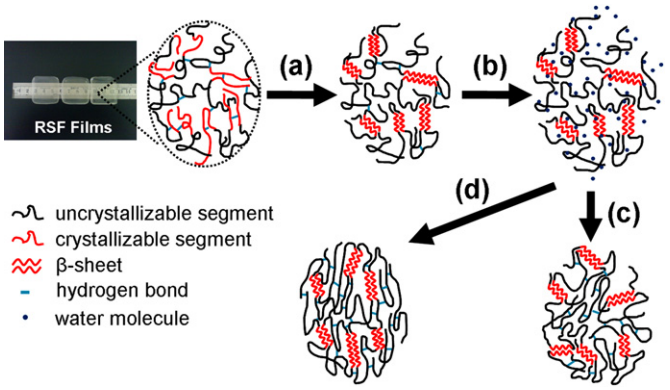

Scheme 1. Brief illustration of structural transitions of RSF films that experienced (a) ethanol-induced crystallization, (b) hydration via humidity equilibrium, (c) thermal dehydration, and (d) stretching-induced orientation followed by thermal dehydration.

into a new glassy state after thermal dehydration, as the uncrystallizable segments reorganized into more stable structure with a new T_g at as high as 190 °C. Moreover, oriented β-sheet domains of stretched RSF films functioned as physical crosslinking points for the disordered domains. Then the local motility of permanently disordered domains was further limited, which lead to a significantly higher T_g at around 205 °C, quite close to that of silk fiber (219 °C). These findings may explain the disparities among those reported data of fibroin glass transition in literatures.

4. Conclusion

As a structural biomacromolecule, silk fibroin has a complex fine structure responsible for its glass transition reported in a wide range of 150–250 °C in literatures since 1980s. However, the structural details underlying the segmental movements of silk fibroin are still unclear due to the lack of appropriate characterization tools. In this paper, DMA was particularly applied as "thermal fingerprint" to correlate dynamic tan δ results with structural changes in RSF films during crystallization, thermal dehydration and orientation, respectively. The results suggested that DMA is an effective method for the insight into the microstructure of RSF, which would guide the fabrication of RSF based materials with high mechanical performance such as annealed artificial fiber and post-stretched film.

Acknowledgement

This work was supported by the National Natural Science Foundation of China (NSFC 20974024 and 21034003), and 973 Project of Chinese Ministry of Science and Technology (No. 2009CB930000). The authors acknowledge Dr. Yong Yang for the DMA measurement of silk fiber, and give special thanks to Dr. David Porter from Oxford University as well as Ms. Jianwei Yin and Dr. Chengjie Fu from Fudan University for constructive suggestions.

Appendix. Supplementary material

Supplementary data associated with this article can be found in the online version, at doi:10.1016/j.polymer.2010.10.046.

References

[1] Nakamura S, Magoshi J, Magoshi Y. In: Kaplan DL, Adams WW, Farmer B, Viney C, editors. Silk polymers: materials science and biotechnology, ACS symposium series, vol. 544. American Chemical Society; 1994. pp. 211–221.
[2] Vepari C, Kaplan DL. Progress in Polymer Science 2007;32(8–9):991–1007.
[3] Hardy JG, Romer LM, Scheibel TR. Polymer 2008;49(20):4309–27.
[4] Jin HJ, Kaplan DL. Nature 2003;424(6952):1057–61.
[5] Sehnal F, Zurovec M. Biomacromolecules 2004;5(3):666–74.
[6] Shen Y, Johnson MA, Martin DC. Macromolecules 1998;31(25):8857–64.
[7] Porter D, Vollrath F. Advanced Materials 2009;21(4):487–92.
[8] Hu X, Kaplan D, Cebe P. Macromolecules 2006;39(18):6161–70.
[9] Hu X, Lu Q, Kaplan DL, Cebe P. Macromolecules 2009;42(6):2079–87.
[10] Jiang CY, Wang XY, Gunawidjaja R, Lin YH, Gupta MK, Kaplan DL, et al. Advanced Functional Materials 2007;17:2229–37.
[11] Huang XT, Shao ZZ, Chen X. Acta Chimica Sinica 2007;65(22):2592–6.
[12] Tsukada M, Gotoh Y, Nagura M, Minoura N, Kasai N, Freddi G. Journal of Polymer Science Part B-Polymer Physics 1994;32(5):961–8.
[13] Motta A, Fambri L, Migliaresi C. Macromolecular Chemistry and Physics 2002;203(10–11):1658–65.
[14] Ki CS, Um IC, Park YH. Polymer 2009;50(19):4618–25.
[15] Magoshi J, Magoshi Y. Journal of Polymer Science Part B-Polymer Physics 1975;13(7):1347–51.
[16] Tsukada M, Freddi G, Gotoh Y, Kasai N. Journal of Polymer Science Part B-Polymer Physics 1994;32(8):1407–12.
[17] Tsukada M, Freddi G, Kasai N, Monti P. Journal of Polymer Science Part B-Polymer Physics 1998;36(15):2717–24.
[18] Kweon HY, Um IC, Park YH. Polymer 2000;41(20):7361–7.
[19] Yang Y, Chen X, Shao ZZ, Zhou P, Porter D, Knight DP, et al. Advanced Materials 2005;17(1):84–8.
[20] Yin JW, Chen EQ, Porter D, Shao ZZ. Biomacromolecules 2010;11:2890–5.
[21] Tsukada M, Freddi G, Kasai N. Journal of Polymer Science Part B-Polymer Physics 1994;32(7):1175–82.
[22] Magoshi J, Nakamura S. Journal of Applied Polymer Science 1975;19(4):1013–5.
[23] Magoshi J, Magoshi Y, Nakamura S. Journal of Applied Polymer Science 1977;21(9):2405–7.
[24] Nakamura S, Saegusa Y, Yamaguchi Y, Magoshi J, Kamiyama S. Journal of Applied Polymer Science 1986;31(3):955–6.
[25] Tsukada M, Freddi G, Nagura M, Ishikawa H, Kasai N. Journal of Applied Polymer Science 1992;46(11):1945–53.
[26] Yang Y, Chen X, Zhou P, Yao WH, Shao ZZ. Chemical Journal of Chinese Universities-Chinese 2001;22(9):1592–6.
[27] Magoshi J, Magoshi Y, Nakamura S, Kasai N, Kakudo M. Journal of Polymer Science Part B-Polymer Physics 1977;15(9):1675–83.
[28] Zhou GQ, Shao ZZ, Knight DP, Yan JP, Chen X. Advanced Materials 2009;21(3):366–70.
[29] Yan JP, Zhou GQ, Knight DP, Shao ZZ, Chen X. Biomacromolecules 2009;11(1):1–5.
[30] Chen X, Knight DP, Shao ZZ, Vollrath F. Biochemistry 2002;41(50):14944–50.
[31] Mo CL, Wu PY, Chen X, Shao ZZ. Applied Spectroscopy 2006;60(12):1438–41.
[32] Agarwal N, Hoagland DA, Farris RJ. Journal of Applied Polymer Science 1997;63(3):401–10.
[33] Mo CL, Wu PY, Chen X, Shao ZZ. Vibrational Spectroscopy 2009;51(1):105–9.
[34] Guadagno L, D'Aniello C, Naddeo C, Vittoria V, Romano G. Journal of Macromolecular Science-Physics 2004;B43(2):349–63.
[35] Guadagno L, Naddeo C, Vittoria V, Meille SV. Macromolecules 2005;38(21):8755–64.
[36] Yuan QQ, Yao JR, Chen X, Huang L, Shao ZZ. Polymer 2010;51(21):4843–9.
[37] Hu X, Kaplan D, Cebe P. Macromolecules 2008;41(11):3939–48.
[38] Plaza GR, Guinea GV, Perez-Rigueiro J, Elices M. Journal of Polymer Science Part B-Polymer Physics 2006;44(6):994–9.
[39] Hu X, Kaplan D, Cebe P. Thermochimica Acta 2007;461(1–2):137–44.
[40] Fu CJ, Porter D, Shao ZZ. Macromolecules 2009;42(20):7877–80.
[41] Khan AN, Hong PD, Chuang WT, Shih KS. Polymer 2009;50(26):6287–96.